International Journal of Engineering and Technology Innovation, vol. 16, no. 3, 2026, pp. 396-413

Superstructure Inertia Effects on Lateral Impact Response and Failure Prediction of Axially Loaded RC Columns

Xiaoyuan Song [1], Guang Li [1], Qianqian Zhai [1], Jingming Sun[1,3,*], Mengsi Yu [2], Min Li [2], Guangyuan Ni [2], Ben Chen[2]

[1]School of Civil Engineering and Architecture, Linyi University, Linyi, China

[2]Jinzhongzheng Project Management Co., Ltd, Linyi, China

[3]College of Civil Engineering, Hunan University, Changsha, China

Received 07 June 2026; revised 30 June 2026; accepted 08 July 2026

DOI: https://doi.org/10.46604/ijeti.2026.16507

Abstract

This study aims to investigate the influence of axial loading representation and superstructure inertia on the lateral impact response and failure prediction of axially loaded reinforced concrete (RC) columns. A validated LS-DYNA finite element model, calibrated against pendulum impact tests, is used to compare three axial loading schemes: lever loading, mass loading, and constant force loading for 15 column cases with different loading conditions and failure modes. The results show that the axial loading representation has limited influence on the initial impact-force peak but strongly affects the impact-force plateau, displacement response, residual deformation, and damage pattern. The mass loading model agrees well with the lever loading model, whereas the constant force model underestimates the impact-force plateau and overestimates peak and residual displacements. Relative to the mass loading model, the constant force model yields average ratios of 0.876, 1.107, and 1.177 for the impact-force plateau, peak displacement, and residual displacement, respectively.

Keywords: reinforced concrete column, lateral impact, superstructure inertia, axial loading model

1. Introduction

Reinforced concrete (RC) columns are critical vertical load-bearing components in buildings, bridge piers, underground parking structures, and transportation infrastructure. Their dynamic response and damage evolution under accidental lateral impact loads directly affect the safety and progressive collapse resistance of structural systems. In recent years, increasing attention has been paid to the risk of severe damage to RC members and bridge piers induced by low-velocity impact, vehicle collision, rockfall impact, blast loading, and other accidental dynamic events [1–9]. Under short-duration, high-intensity dynamic loading, axially loaded RC columns may exhibit complex nonlinear responses, including flexural deformation, shear damage, concrete crushing, reinforcement yielding, and residual deformation. Unlike conventional static or quasi-static loading conditions, the response of RC columns subjected to lateral impact depends not only on the impact mass, impact velocity, reinforcement detailing, and boundary constraints, but also on the dynamic transfer mechanism of axial load during impact. Therefore, accurately elucidating the dynamic response and failure of axially loaded RC columns subjected to lateral impact is of great importance for impact-resistant structural design, post-event safety assessment, and resilience enhancement.

Extensive experimental, numerical, and analytical studies have investigated the dynamic response, damage evolution, and impact resistance of RC and steel-reinforced concrete (SRC) columns subjected to lateral impact. Recent studies have examined the impact behavior and post-impact damage assessment of RC and SRC columns under various collision scenarios

* Corresponding author. E-mail address: gzdxyjssjm@163.com

[2, 3, 6, 10]. Sun et al. [7] investigated the effects of impact mass and velocity on the failure modes of RC columns under lateral impact, while Cengiz et al. [8] examined the dynamic response and residual static performance of axially loaded RC columns subjected to low-elevation impact. Al-Bukhaiti et al. [11] analyzed the influence of axial load on CFRP-confined RC columns under asymmetric lateral impact, and Luan et al. [12] evaluated the residual axial compression capacity of RC columns after lateral impact. Several subsequent studies further investigated the effects of failure mode, impact scenario, axial loading condition, and post-impact damage characteristics on the impact response of RC members and columns [13–17]. These studies have significantly improved the understanding of impact-induced damage and residual performance of RC columns. However, the dynamic representation of axial loading and the associated superstructure inertia effect have not been critically examined. This gap is important because actual columns interact with upper structural masses during impact, whereas a constant axial force boundary may reproduce the initial compression but cannot represent the inertial feedback of the superstructure.

In existing impact tests and finite element analyses of RC columns, axial load is commonly applied using hydraulic jacks, disc springs, upper counterweights, equivalent mass blocks, or constant axial force boundary conditions [7, 8, 10–17]. These methods can provide a prescribed axial compression force initially; however, their ability to reproduce the dynamic axial force transfer process during impact may differ significantly. The constant axial force model can be implemented easily in numerical simulations and is therefore frequently adopted as a simplified boundary condition for representing axial compression. However, RC columns in real structures do not sustain constant axial compression in isolation. Instead, they interact dynamically with upper beams, floor masses, bridge decks, or other superstructure components. When a column is subjected to lateral impact, the mass of the superstructure may generate an inertial response following the motion of the column top, resulting in dynamic fluctuations in the axial force within the column. This dynamic axial force also contributes to impact energy redistribution, compression–flexure interaction, compression–shear interaction, and damage evolution. Therefore, replacing the actual superstructure mass effect with a constant axial force boundary condition may alter key predicted responses, including the impact force plateau, impact duration, peak displacement, residual displacement, and shear damage distribution.

Although several recent numerical studies have considered axial load effects, post-impact residual behavior, and impact-induced force transfer in RC columns and members [8, 11, 12, 15–18], the equivalence of different axial loading representations during lateral impact remains insufficiently clarified. In particular, it is still unclear how the axial load transfer path and column-top inertial feedback affect the predicted impact-force history, axial-force fluctuation, displacement response, residual deformation, and damage pattern. This issue is especially important for shear-controlled and flexure–shear-controlled columns because compression–shear interaction and diagonal damage development are sensitive to axial-force variation. Therefore, a direct comparison of different axial loading representations is needed to identify when a simplified constant-force model is acceptable and when an explicit representation of superstructure inertia is required.

Based on the above considerations, this study develops a refined finite element model of axially loaded RC columns subjected to lateral impact using LS-DYNA and validates the model against existing pendulum impact test results [22]. On this basis, three representative axial loading models are established: the lever loading (LL) model, the mass loading (ML) model, and the constant force loading (NL) model. The LL model simulates the lever-type axial load transfer mechanism adopted in the tests; the ML model accounts for the vertical inertial effect induced by the superstructure mass; and the NL model represents the commonly used constant axial force approach. Their predicted impact-force histories, displacement responses, residual deformations, and final damage states are systematically compared under identical modeling conditions.

Particular attention is paid to whether the inertial effect of the superstructure significantly alters the predicted impact response, which response indicators are most affected by the simplified constant axial force model, and whether the sensitivity to axial loading models varies with failure mode. The results of this study can provide valuable guidance for finite element modeling, equivalent treatment of axial load boundary conditions, and post-impact damage assessment of axially loaded RC columns subjected to lateral impact.

2. Calibration of Impact Force in the Test

In pendulum and drop-weight impact tests, the impact force is commonly measured using a force sensor installed in the hammer head or within the loading device. However, the recorded force is not always identical to the actual contact force between the hammer head and the specimen. Previous studies have shown that the installation position of the force sensor in the impact device can affect the measured impact force, particularly when it is located directly at the contact interface between the hammer head and the specimen. In such cases, the measured force may be influenced by the hammer's mass distribution and local inertial effects [21]. Therefore, before validating a finite element model using experimentally measured impact force, it is necessary to clarify the relationship between the sensor-measured force and the actual contact force.

In the pendulum impact tests used in this study, the force sensor was installed at the rear of the pendulum hammer head, rather than directly at the contact interface [22]. A simplified mechanical model of the pendulum system is shown in Fig. 1. With this arrangement, the sensor mainly measures the interaction between the rear counterweight mass and the hammer head, while the actual contact force also includes the inertial contribution of the hammer head during impact. If the sensor's reading is directly used as the contact force, the impact magnitude may be underestimated. This underestimation can affect the validation of contact stiffness, damage evolution, and displacement response in the finite element model. For this reason, the pendulum impact force was first calibrated in this study. The corrected actual contact force was then adopted as a reference for comparison in the finite element analysis.

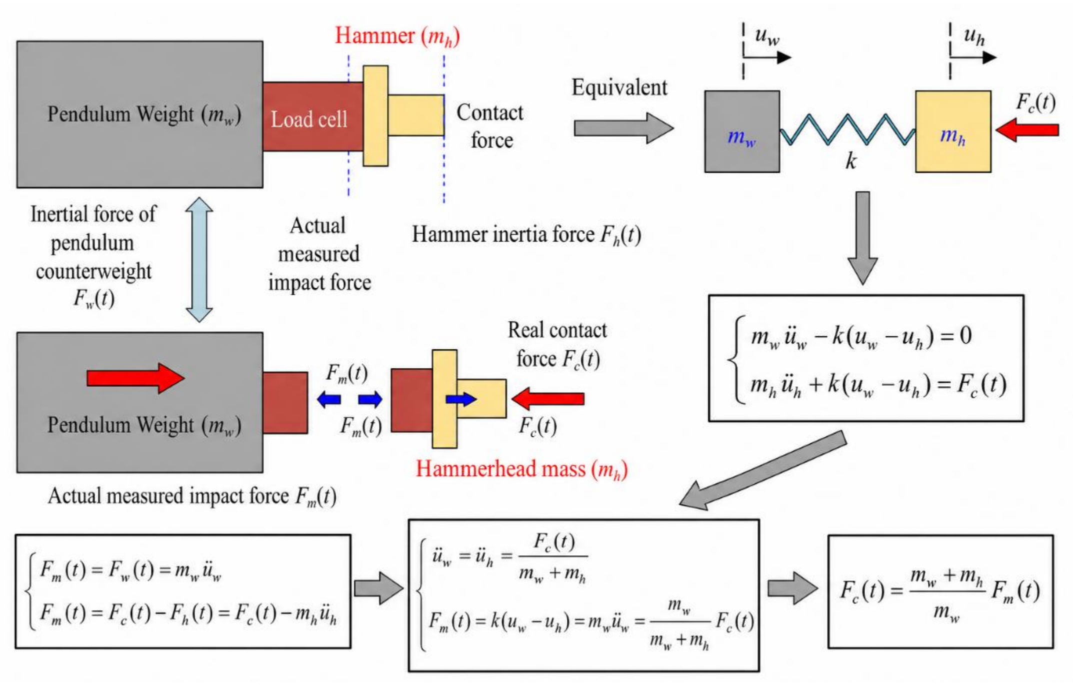

Fig. 1 Simplified mechanical model of the pendulum mass system

To establish the conversion relationship between the measured impact force and the actual contact force, the pendulum system was simplified as a mass-transfer system consisting of the rear counterweight mass, the hammer head mass, and the force sensor represented by an equivalent spring, as shown in Fig. 1. The pendulum counterweight mass behind the force sensor is denoted as m_w, the equivalent mass of the hammer head is denoted as m_h, the force sensor is modeled as an axial elastic element, the measured force is denoted as F_m(t), and the actual contact force between the hammer head and the specimen is denoted as F_c(t). Because the overall stiffness of the hammer head is much higher than that of the RC column specimen, and no obvious deformation of the hammer head was observed during impact, it can be reasonably assumed that the hammer head and the main body of the pendulum move synchronously during the impact stage, namely, they share the same instantaneous acceleration. This assumption is adopted as an engineering approximation for the present pendulum impact system.

First, the rear counterweight mass, load cell, and hammer head were connected in series through a compact steel assembly, and the stiffness of these steel components was much higher than that of the RC column specimen. Second, no visible deformation or plastic damage to the hammer head or loading assembly was observed after the tests. Third, the global response of interest in this study is the contact force history at the structural-member time scale, rather than the local high-frequency vibration of the sensor–hammer subsystem. Therefore, the relative motion between the rear counterweight mass and the hammer head is expected to be much smaller than the global deformation of the impacted RC column during the main impact stage. Based on these considerations, the measured force is corrected using a first-order approximation that accounts for the mass distribution of the pendulum system.

According to D'Alembert's principle, the dynamic equilibrium equations were established separately for the rear counterweight mass of the pendulum and the hammer head mass. For the counterweight mass behind the force sensor, the relationship between the inertial force and the force measured by the sensor can be expressed as:

$$F_m(t) = m_w \ddot{u}_w(t) \tag{1}$$

For the hammer head mass, the actual contact force consists of the force transmitted by the force sensor and the inertial force of the hammer head, which can be expressed as:

$$F_c(t) = F_m(t) + m_h \ddot{u}_h(t) \tag{2}$$

where $\ddot{u}_w(t)$ and $\ddot{u}_h(t)$ are the instantaneous accelerations of the rear counterweight mass of the pendulum and the hammer head mass, respectively. Since the rear counterweight mass and the hammer head approximately move synchronously during the impact process, the following relationship can be adopted:

$$\ddot{u}_w(t) = \ddot{u}_h(t) \tag{3}$$

By substituting the above relationship, the conversion relationship between the actual contact force and the force measured by the sensor can be obtained as:

$$F_c(t) = \frac{m_w + m_h}{m_w} F_m(t) \tag{4}$$

It can be seen from the equation that, when the force sensor is installed behind the hammer head, the measured impact force F_m(t) represents only the inertial response associated with the rear counterweight mass of the pendulum, whereas the actual contact force F_c(t) also includes the inertial contribution generated by the participation of the hammer head mass in the impact process. Therefore, the actual contact force is generally greater than the impact force directly measured by the force sensor, and the magnitude of the correction depends on the relative proportion between the hammer head mass and the rear counterweight mass.

It should be noted that the synchronous-acceleration assumption does not imply a perfectly rigid connection between the hammer head and the rear counterweight mass. Local compliance of the load cell and hammer assembly may induce a small phase difference or high-frequency oscillation, particularly near the initial impact peak. Therefore, the corrected force should be interpreted as an approximate representation of the actual contact force at the structural response scale. This approximation may slightly influence the amplitude of the initial peak and local oscillatory components of the force history, but it has limited influence on the overall plateau, impact duration, and unloading trend used for finite element validation. Moreover, the finite element model was validated using not only the corrected impact force but also the displacement response, axial-force variation, and final damage pattern, which reduces the sensitivity of the validation to this single correction assumption.

Fig. 2 compares the time history curves of the impact force measured by the force sensor and the corrected actual contact force for representative specimens. The two curves show good agreement in their overall trends, and both capture the characteristics of the initial impact peak, plateau stage, and unloading stage. This indicates that the signal measured by the force sensor accurately reflects the temporal evolution of the impact process. However, in terms of force magnitude, the corrected actual contact force is higher than the measured impact force, suggesting that the inertial contribution of the hammer head mass affects the contact force amplitude. If this inertial correction is neglected, the actual impact force between the hammer head and the specimen may be underestimated.

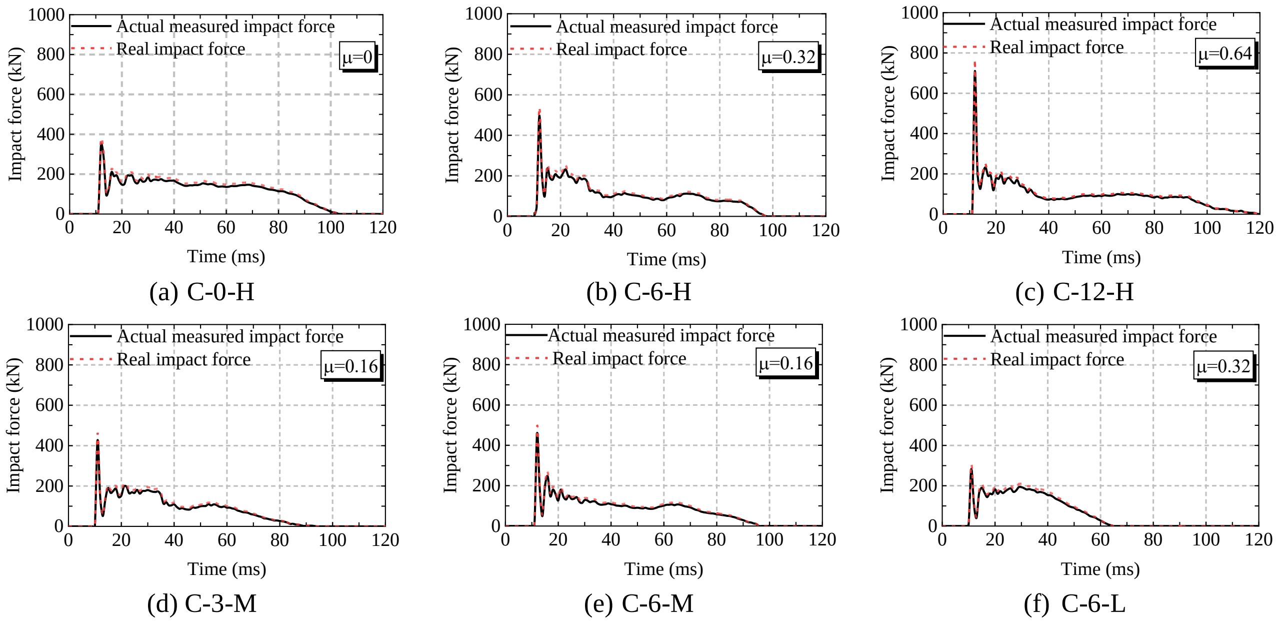

Fig. 2 Comparison between the measured impact force and the corrected contact force

Based on the above analysis, the force measured directly by the force sensor is not used for the subsequent validation of the finite element model. Instead, the actual contact force corrected for mass distribution is adopted as the evaluation metric for the impact force. This treatment improves the consistency between the experimental data and the finite element results and serves as the basis for subsequent comparisons of the impact force plateau, impact duration, and damage response of RC columns under different axial loading methods.

3. Numerical Simulation

3.1 Numerical Geometric Model Information

To investigate the influence of the superstructure inertial effect on the lateral impact response and failure prediction of axially loaded RC columns, a refined finite element model of RC columns subjected to pendulum impact was developed using LS-DYNA. The geometric dimensions, loading device layout, boundary conditions, and initial impact parameters were kept consistent with those of the existing pendulum impact tests. Detailed information on the tests can be found in [22]. The finite element model comprises the column specimen, foundation beam, top beam, distribution beam, clamping beams, spherical hinge, force sensor, lever loading device, hanging basket counterweight, prestressed tie rods, steel cables, and the pendulum system. The model was established at a 1:1 scale relative to the experimental prototype to ensure that the numerical model could realistically reproduce the experimental loading path and dynamic response characteristics of the structural components.

Figure 3 shows the overall finite element model. The concrete column specimen, foundation beam, top beam, distribution beam, clamping beams, spherical hinge, force sensor, lever device, pin shafts, hanging basket counterweight, and pendulum were all simulated using three-dimensional eight-node solid elements. The longitudinal reinforcement and stirrups were modeled using Hughes–Liu beam elements to capture their tensile, compressive, flexural, and plastic deformation behavior under impact loading. The prestressed tie rods and suspension cables were modeled using discrete beam or cable elements, with the cables assumed to resist only tension and to carry no compressive force, consistent with the actual mechanical behavior of the flexible suspension system used in the tests. In the column specimen, the reinforcement and concrete were modeled using a shared-node approach, whereas the interaction between reinforcement and concrete in the foundation beam and top beam was established by embedding beam elements into solid elements, thereby ensuring composite action between the reinforcement and concrete.

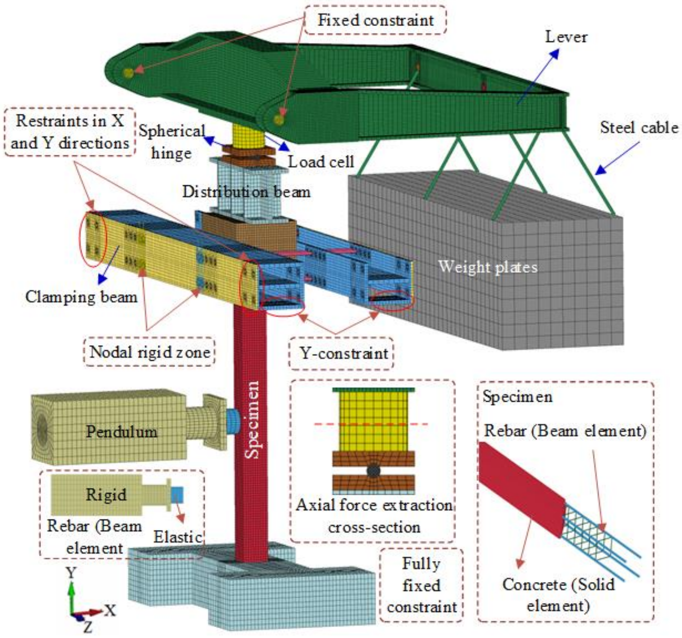

Fig. 3 Finite element model for numerical simulation

In the lever-loading model, the axial compression at the column top was transferred to the column specimen via the hanging-basket counterweight, steel cables, lever, spherical hinge, and distribution beam. This loading method not only provides the required initial axial compression but also captures the dynamic axial load transfer of the counterweight and lever systems during lateral impact. The initial axial compression in the finite element model was kept consistent with the prescribed experimental value by adjusting the mass density of the hanging basket counterweight. To facilitate the subsequent analysis of axial force variations within the column, an axial force extraction region was defined at a specified section of the column shaft to obtain the time history response of the axial force during the impact process.

The boundary conditions of the model were established to reproduce the experimental setup. Fully fixed constraints were applied to the bolt-hole regions at the bottom of the foundation beam to simulate the rigid connection between the specimen base and the reaction system. Displacement constraints were applied to the bottom of the clamping beams and the lateral restraint positions, to ensure that the column-top loading and restraint conditions were consistent with those in the test. Fixed constraints were assigned to the pin shaft of the support frame to simulate the lever support point. The lateral impact was applied to the pendulum by prescribing an initial velocity. Gravity was also included throughout the model to capture the effects of the self-weight of the specimen, the loading device, and the counterweight system on the initial stress state.

To ensure both computational accuracy and efficiency, a refined mesh was adopted for the column specimen and the impact contact region. The concrete element size in the column shaft was set to 20 mm. The reinforcement element nodes were arranged to be compatible with the concrete mesh to avoid significant influence of local mesh incompatibility on the impact response. The mesh size was selected considering the column cross section, reinforcement arrangement, local contact region, and computational cost of the explicit dynamic analysis. It was considered adequate for capturing the global flexural deformation, local impact damage, and diagonal damage development of the RC column while maintaining acceptable computational efficiency. For the pendulum, loading device, and steel components, appropriate mesh discretization schemes were adopted according to their geometric dimensions and mechanical characteristics. The adopted mesh scheme was validated against the experimental results and subsequently used in the comparative analyses of different axial loading models.

3.2 Material Models and Parameters

In the finite element model, appropriate material models were selected for each component based on its mechanical characteristics and deformation requirements. The longitudinal reinforcement and stirrups in the column specimen were simulated using the *MAT_PIECEWISE_LINEAR_PLASTICITY material model. This model describes the elastoplastic deformation, strain hardening, and failure behavior of reinforcement under impact loading while accounting for the influence of strain-rate effects on the dynamic yield strength of steel reinforcement. The dynamic yield strength of the reinforcement was modified according to the Cowper–Symonds relationship:

$$f_{yd} = f_y[1+(\frac{\dot{\varepsilon}}{C})^{1/P}] \tag{5}$$

where f_{yd} is the dynamic yield strength of the reinforcement; f_y is the static yield strength of the reinforcement; $\dot{\varepsilon}$ is the strain rate; and C and P are the strain-rate parameters. In this study, C and P were taken as 7.274×10^7 and 11.22, respectively. The density, elastic modulus, Poisson's ratio, and failure strain of the reinforcement were set to 7850 kg/m³, 206 GPa, 0.3, and 0.2, respectively. The material parameters of the reinforcement in the foundation beam and top beam were determined according to [22].

Concrete was simulated using the continuous surface cap model, implemented as the *MAT_CSCM_CONCRETE model. This model accounts for concrete crushing, cracking, shear damage, stiffness degradation, and strain-rate effects under complex stress states and is suitable for nonlinear dynamic analysis of RC members subjected to impact and collision loads. In the CSCM model, the failure surface is governed jointly by stress invariants and the cap hardening parameter, and the failure surface function can be expressed as:

$$f(I_1, J_2, J_3) = J_2 - \Re^2(J_3)F_f^2(I_1)F_c(I_1, \kappa) \tag{6}$$

where I_1 is the first invariant of the stress tensor; J_2 and J_3 are the second and third deviatoric stress invariants, respectively; $\Re(J_3)$ is the three-invariant strength reduction function; $F_f(I_1)$ is the failure surface function on the compressive meridian; $F_c(I_1, \kappa)$ is the cap hardening function; and κ is the cap hardening parameter. This model effectively captures tensile–compressive strength asymmetry, compression–shear interaction, and damage accumulation characteristics of concrete under impact loading.

In this study, concrete was simulated using the user-defined parameters of CSCM 159, and the main parameters are listed in Table 1. The concrete parameters were determined according to the measured concrete strength, the specimen information in [22], and the calibrated CSCM parameter set for RC members under impact loading. The strain-rate effect of concrete was considered because impact loading may increase the apparent tensile and compressive resistance of concrete and affect cracking, crushing, and shear damage development.

Table 1 Parameter values of the CSCM model (unit: Pa, m, s)

Parameter	Value	Parameter	Value	Parameter	Value	Parameter	Value	Parameter	Value
RO (kg/m3)	2,400	NPLOT	1	INCRE	0	IRATE	0	ERODE	0
RECOV	0	ITRETRC	0	PRED	0	G(Pa)	1.078E10	K(Pa)	1.181E10
NH	1.0	CH	0	α(Pa)	1.375E7	θ(Pa-1)	0.2884	λ(Pa)	1.051E7
β(Pa-1)	1.929E-8	α1(Pa)	0.7473	θ1(Pa-1)	1.271E-9	λ1(Pa)	0.17	β1(Pa-1)	7.493E-8
α2(Pa)	0.66	θ2(Pa-1)	7.493E-8	λ2(Pa)	0.16	β2(Pa-1)	7.493E-8	R	5
XD (Pa)	8.85E7	W	0.05	D1(Pa-1)	2.5E-10	D2(Pa-2)	3.492E-19	B	1E2
GFC(Pa*m)	5.410E3	D	0.1	GFT(Pa*m)	2.7915E1	GFS(Pa*m)	2.7915E1	pwrc	5
pwrt	1	pmod	1	η0c	1.003E-4	Nc	0.78	η0t	5.781E-5
Nt	0.48	overc(Pa)	1.981E+7	overt(Pa)	1.981E+7	Strate	1	repow	1

For the steel components in the loading device, including the hammer head, pin shaft of the support frame, support frame, force sensor, spherical hinge, distribution beam, and clamping beams, no obvious plastic deformation was observed during the tests, and their stiffness was much higher than that of the RC column specimen. Therefore, these components were simulated using the *MAT_ELASTIC material model with a density of 7,850 kg/m^3, an elastic modulus of 206 GPa, and a Poisson's ratio of 0.3. The main body of the pendulum and the hanging-basket counterweight were primarily used to provide the impact mass and axial loading mass, respectively, and their deformation had limited influence on the response of the specimen. Therefore, they were simulated using the *MAT_RIGID model. The equivalent densities were determined from their actual masses and geometric volumes to ensure consistency with the experimental mass distribution.

The pendulum impact was applied by prescribing an initial velocity using *INITIAL_VELOCITY_GENERATION, and gravity was applied to the entire model using *LOAD_BODY_Y to account simultaneously for the effects of the self-weight of the specimen, loading device, and hanging-basket counterweight on the initial stress state. In the test, the axial load was transferred from the hanging-basket counterweight to the column top via the steel cables, lever, spherical hinge, and distribution beam. In the finite element model, the initial axial compression was controlled by adjusting the density of the hanging-basket counterweight, thereby ensuring consistency between the initial axial force in the numerical model and that in the test. The prestressed tie rods were connected to the steel flange at the end of the clamping beam using *CONSTRAINED_NODAL_RIGID_BODY. The steel cables were simulated using discrete beam or cable elements with tension-only behavior to reflect the mechanical characteristic that actual steel wire ropes cannot resist compression.

The contact definition significantly influences the simulated impact response. The interactions between the hammer head and the column specimen, between the clamping beams and the column top beam, and among the components of the loading device were all defined using *CONTACT_AUTOMATIC_SURFACE_TO_SURFACE. Hard contact was adopted in the normal direction, and the Coulomb friction model was used in the tangential direction. The friction coefficient between the clamping beams and the column top beam was set to 0.02 to maintain consistency with the experimental boundary conditions. The support frame, steel cables, and hanging-basket counterweight were connected using a shared-node approach to ensure stable transmission of the axial force along the experimental loading path.

The boundary conditions were defined according to the experimental setup. Fixed constraints were assigned to the pin shaft of the support frame to represent the lever support point. Displacement constraints were applied to the bottom of the clamping beams and the lateral restraint positions, respectively. Fully fixed constraints were imposed on the bolt-hole regions at the bottom of the foundation beam to simulate the connection between the specimen and the reaction pedestal. In the column specimen, the reinforcement and concrete were modeled using a shared-node approach, assuming deformation compatibility during impact. In the foundation beam and top beam, the interaction between reinforcement and concrete was defined using *CONSTRAINED_BEAM_IN_SOLID.

3.3 Model Validation

To validate the reliability of the developed finite element model, the numerical simulation results were compared with the existing pendulum impact test results. The validation mainly included the impact force time history curves, lateral displacement time history curves, and final damage patterns. Considering the influence of the force sensor installation position on the measured impact force, the corrected actual contact force described in Section 1 was adopted for the impact force validation.

Fig. 4 compares the experimental and finite element simulation results of the impact force time history curves for representative specimens. The finite element model reproduces the characteristic initial impact peak, plateau, and unloading stages. The simulated peak impact forces for different specimens generally agree well with the experimental results, indicating that the contact stiffness between the hammer head and the specimen, the pendulum's mass distribution, and the initial impact velocity in the model were appropriately defined. Certain deviations can be observed in the impact force plateau stage for some specimens, which may be attributed to the local flexibility of the loading device, friction at the contact interface, boundary gaps, and the inherent randomness of local concrete damage evolution during the tests. Overall, the finite element model can accurately capture the time history characteristics of the contact force during the lateral impact process of RC columns.

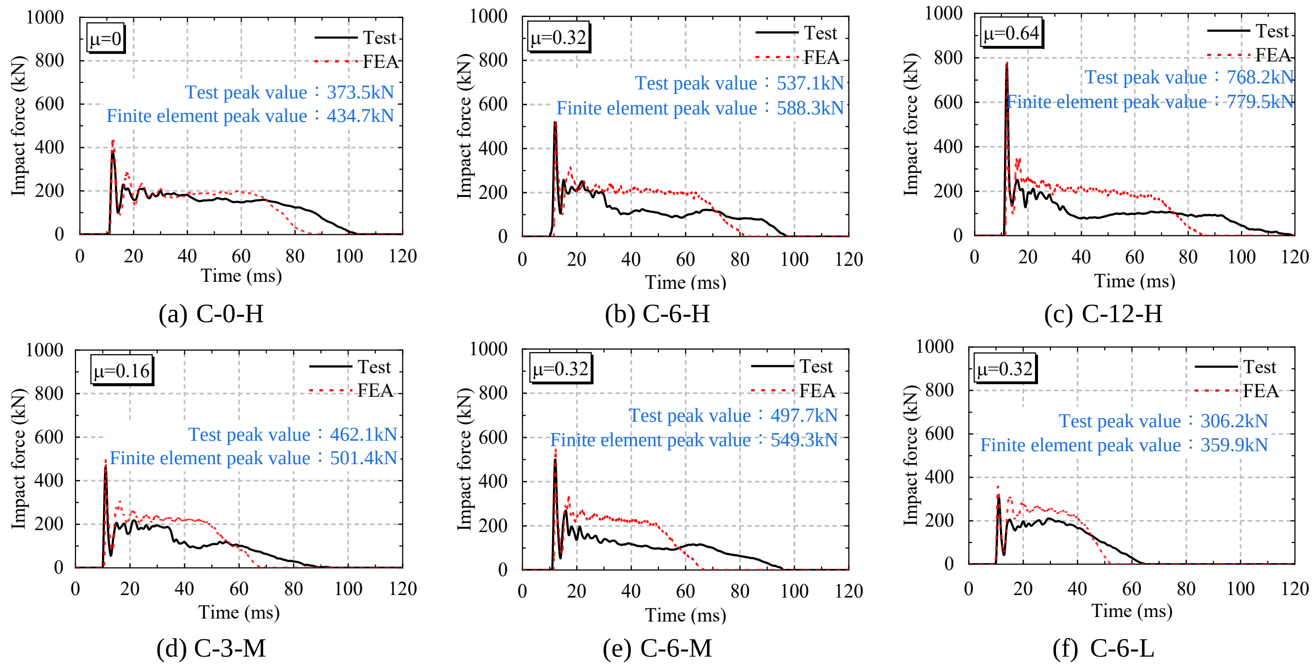

(a) C-0-H (b) C-6-H (c) C-12-H

(d) C-3-M (e) C-6-M (f) C-6-L

Fig. 4 Comparison of impact force time-history curves

Fig. 5 compares the experimental and simulated lateral displacement time history curves. The finite element model reasonably predicts the displacement rising stage and peak displacement, indicating that it can capture the global dynamic deformation of RC columns under impact loading. Certain discrepancies are observed during the unloading and residual displacement stages, mainly due to the simplified modeling of the loading device, the neglect of bond slip between reinforcement and concrete, and the idealized boundary conditions. Overall, the model provides an acceptable prediction of the displacement response.

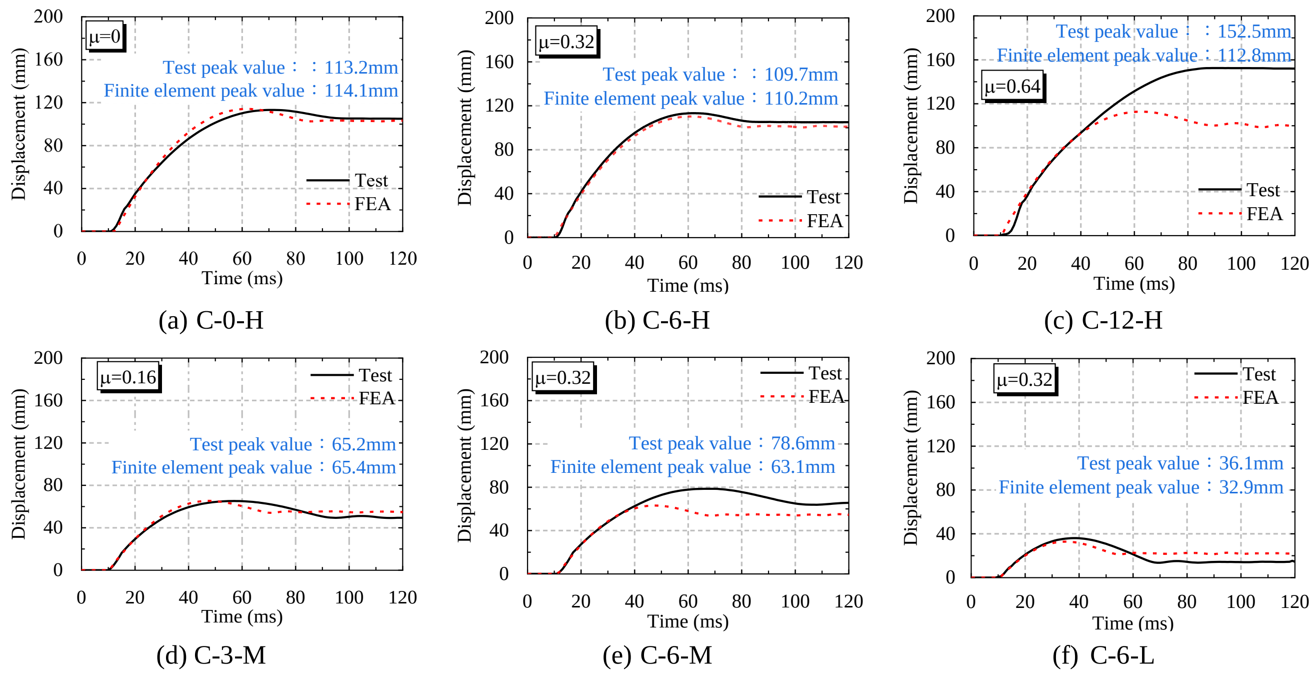

(a) C-0-H (b) C-6-H (c) C-12-H

(d) C-3-M (e) C-6-M (f) C-6-L

Fig. 5 Comparison of displacement time-history curves

Fig. 6 compares the experimental and finite element simulation results for the axial force time history responses of representative specimens during impact. The finite element model reproduces the dynamic trend of the column axial force during the impact process. Unlike the static axial compression condition, the axial force in the column under lateral impact does not remain constant but fluctuates significantly with the column's lateral deformation, inertial response, and the dynamic force transfer process of the loading system. The simulation results reproduce the rapid disturbance in axial force during the initial impact stage and the subsequent attenuation of oscillation, indicating that the axial force transfer path among the lever-loading system, the hanging-basket counterweight, the steel cables, and the column-top distribution beam was appropriately defined in the model. Owing to the flexibility, friction, and local gaps in the experimental loading device, certain differences can be observed between the experimental and simulated results, particularly in axial force peaks and oscillation amplitudes for some specimens. Nevertheless, the overall trend of variation remains consistent, indicating that the developed lever-loading model provides a reliable benchmark for subsequent comparisons with the mass-loading and constant-force loading models.

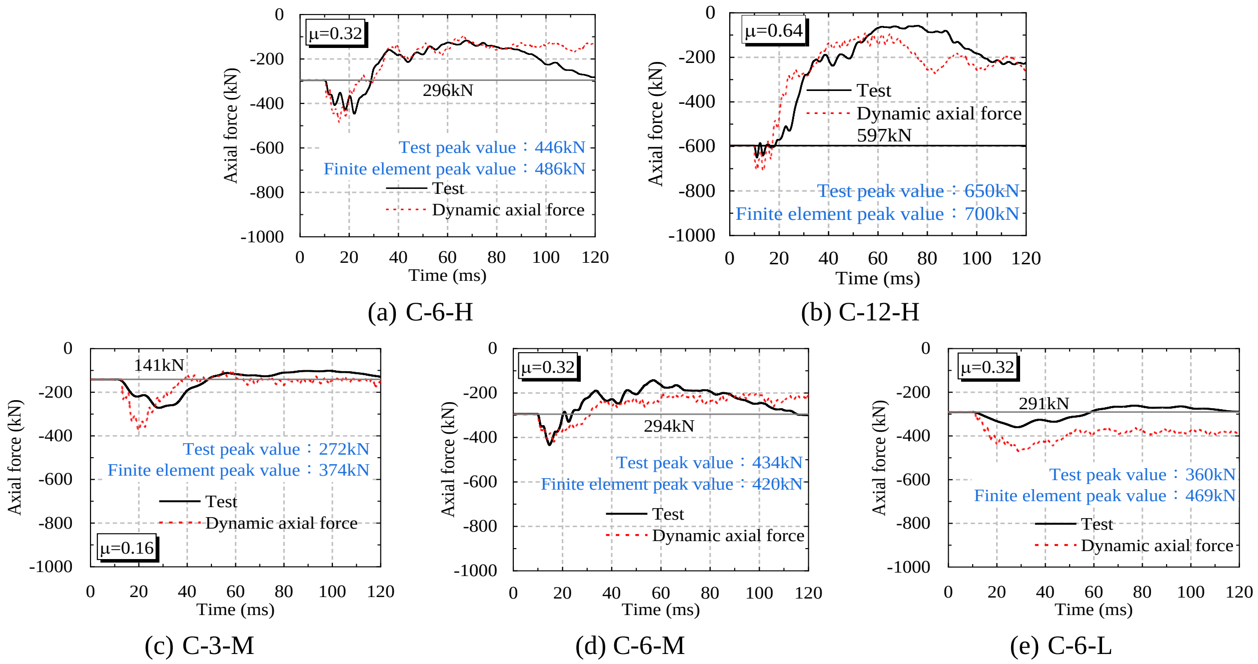

Fig. 6 Axial force variation curves

To further quantify the predictive accuracy of the numerical model, the mean absolute peak-value errors were calculated for the representative specimens shown in Figs. 4–6. The corresponding errors of the impact force, lateral displacement, and axial force are approximately 10.7%, 9.4%, and 17.5%, respectively. The relatively larger error in the axial-force response is mainly attributed to the flexibility, friction, and local gaps of the experimental loading system, as well as the sensitivity of axial-force fluctuation to boundary conditions during impact. Overall, these quantitative indicators further confirm that the finite element model can reasonably reproduce the main impact response of the tested RC columns and can be used for the subsequent comparison of different axial loading methods.

Fig. 7 further compares the experimental damage patterns with the finite element damage contours. The finite element model reproduces the main failure characteristics of the specimens. For specimens governed by flexural failure, the simulation results can reflect the damage concentration near the column end or impact region as well as the overall flexural deformation characteristics. For specimens governed by shear or flexure–shear failure, the model can capture concrete crushing in the impact region, the development of diagonal damage bands, and the tendency toward localized shear failure. The main crack distributions and failure modes observed in the tests agree well with the finite element damage distributions, indicating that the adopted concrete CSCM model, elastoplastic reinforcement model, and contact boundary conditions can reasonably describe the damage evolution of RC columns subjected to lateral impact.

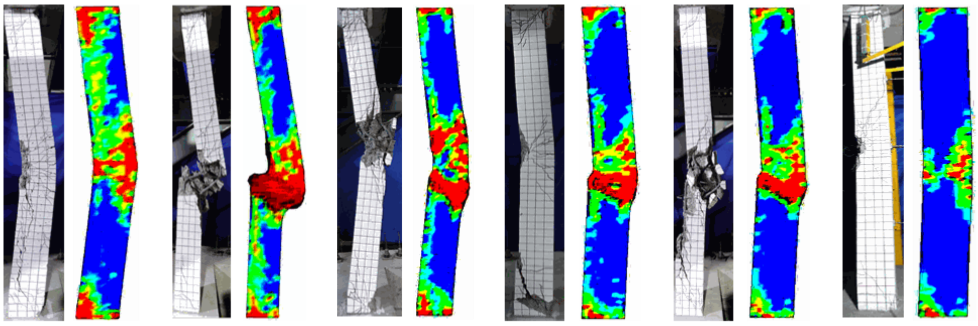

(a) C-0-H (b) C-6-H (c) C-12-H (d) C-3-M (e) C-6-M (f) C-6-L

Fig. 7 Comparison of experimental and finite element damage patterns

4. Effect of Axial Loading Methods on the Impact Resistance of RC Columns

4.1 Finite Element Models for Different Axial Loading Methods

Based on the validated lever-loading model, two additional axial loading models were established to investigate the influence of superstructure inertia on the lateral impact response and failure prediction of axially loaded RC columns. The three models are defined as the lever loading (LL), mass loading (ML), and constant force loading (NL) models. The LL model retains the experimental axial load transfer system and serves as the benchmark model. The ML model replaces the lever mechanism with an equivalent mass block at the column top to represent the vertical inertial effect of the superstructure, as shown in Fig. 8(a). In contrast, the NL model applies a constant axial compression directly to the column top, as shown in Fig. 8(b), and therefore neglects the dynamic interaction between the column and the superstructure mass.

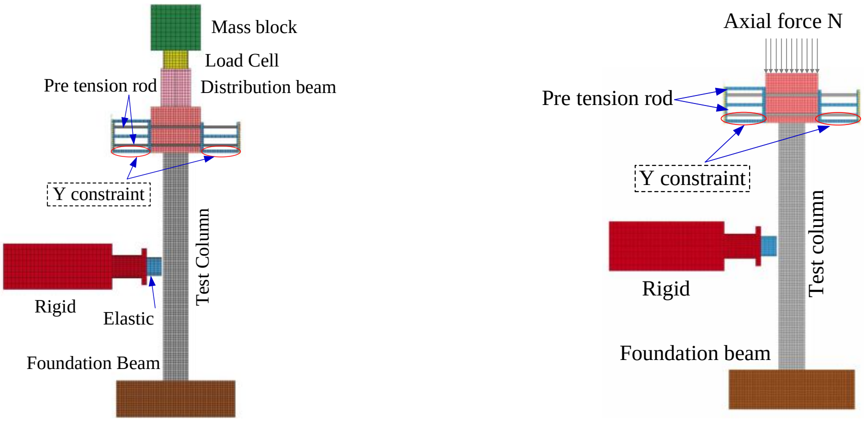

(a) Axial load application via mass block (b) Axial load application via force boundary

Fig. 8 Finite element models with different axial load application methods

To ensure a meaningful comparison, the geometric dimensions, material parameters, contact interactions, boundary conditions, mesh size, initial impact velocity, impact mass, and initial axial compression were kept identical for the LL, ML, and NL models, except for the axial loading method. Thus, the differences in the numerical results mainly result from the axial force transfer mechanism and the inertial participation of the superstructure mass. Fifteen RC column cases with different axial compression levels, impact masses, impact velocities, and failure modes were selected and denoted as A1–A3, B1–B3, and C1–C9, with the corresponding specimen designations provided in Figs. 9, 11, and 13. These cases cover low to relatively high axial compression levels, different impact intensities, and representative flexural, shear, and flexure–shear responses, allowing the influence of axial loading representation to be examined under practically relevant failure conditions.

4.2 Effect of Impact Force

To reveal the influence of axial loading models on the predicted lateral impact contact force of RC columns, 15 column cases were analyzed using the LL, ML, and NL models. Fig. 9 presents the impact force time history curves, while Fig. 10

quantifies the differences in impact duration t_d and impact force plateau F_p between the LL/NL models and the ML model. Because the ML model includes the inertial degrees of freedom of the superstructure mass while maintaining the same initial axial compression, it is used as the reference model for evaluating the LL model and the simplification error of the NL model.

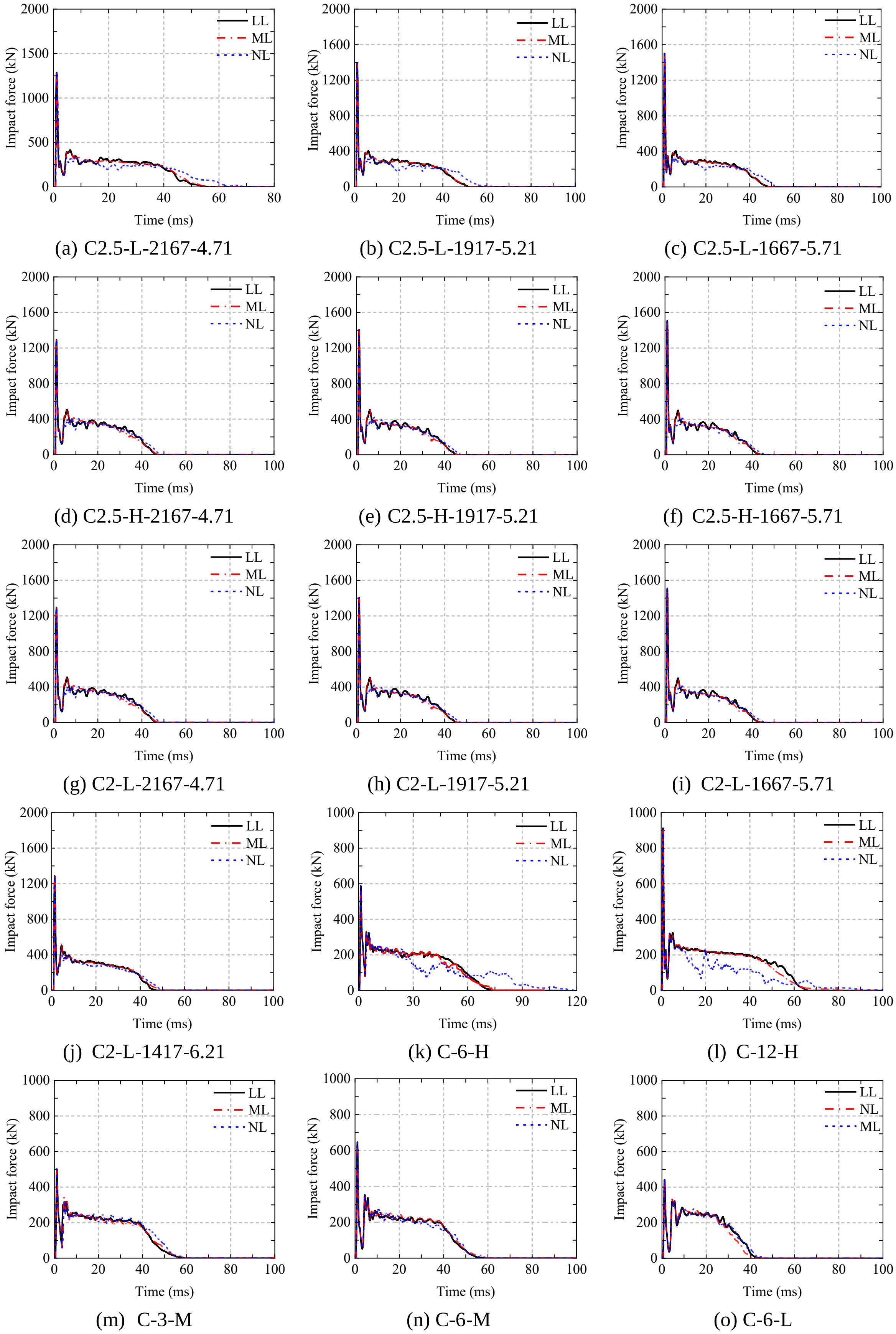

Fig. 9 Comparison of LL, ML, and NL impact force time-history curves

As shown in Fig. 9, the three models predict similar initial impact force peaks, indicating that the initial peak is mainly governed by local contact stiffness, impact mass, impact velocity, and the compressive response of concrete in the contact region. However, clear differences appear during the impact plateau stage. The LL and ML models show good agreement in both F_p and t_d, suggesting that the mass loading model can reasonably represent the dynamic axial force transfer mechanism of the lever loading system. In contrast, the NL model predicts a lower impact force plateau and a different impact duration, particularly for shear-controlled specimens such as A1–A3. This is because the constant force model neglects the vertical inertial response of the superstructure mass and weakens the dynamic coupling between axial load and lateral impact response.

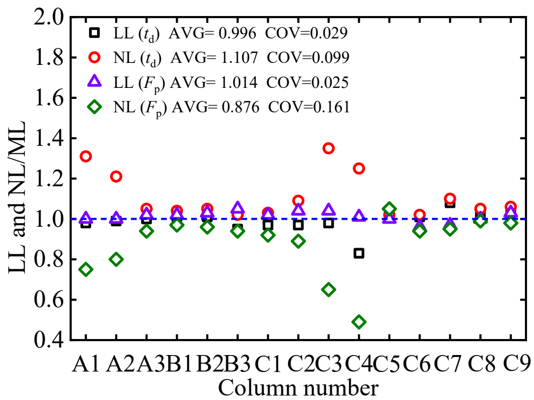

Fig. 10 Comparison of the differences in t_d and F_p between the LL, NL, and ML loading models

Fig. 10 further confirms these observations. For the LL model relative to the ML model, the mean ratios of t_d and F_p are 0.996 and 1.014, with coefficients of variation of 0.029 and 0.025, respectively, indicating high consistency between the two models. In contrast, the mean F_p ratio of the NL model relative to the ML model is approximately 0.876, with a coefficient of variation of 0.161, showing that the NL model tends to underestimate the impact force plateau and produces greater dispersion among different cases. Therefore, although the axial loading model has limited influence on the initial impact peak, it significantly affects the impact plateau and duration, especially for shear-dominated responses. This finding is generally consistent with previous studies showing that the impact response of axially loaded RC columns is strongly affected by axial load level, impact mass, impact velocity, and failure mode. However, the present results further indicate that the axial loading representation itself can influence the predicted response even when the same initial axial force is applied. The difference occurs because the LL and ML models allow dynamic axial-force fluctuation and inertial feedback from the loading system or column-top mass, whereas the NL model maintains a constant axial force and therefore weakens the coupling between axial compression and lateral impact response.

4.3 Effect of Displacement Response

To further evaluate the influence of axial loading models on global deformation and post-impact residual performance, Fig. 11 compares the lateral displacement time-history curves predicted by the LL, ML, and NL models, while Fig. 12 quantifies the differences in peak displacement D_m and residual displacement D_r between the LL/NL models and the ML model. Compared with the impact force response, the displacement response provides a more direct measure of deformation capacity, damage accumulation, and post-impact residual performance.

As shown in Fig. 11, the three models show only minor differences during the initial stage of displacement development because the response is mainly controlled by impact input energy, initial stiffness, boundary constraints, and global inertia. As nonlinear damage develops, the effect of the axial loading model becomes more evident. The LL and ML models show good agreement, especially in terms of displacement and unloading response, indicating that the ML model can reasonably capture the inertial feedback of the column-top mass. In contrast, the NL model generally predicts larger D_m and D_r, particularly for shear-controlled cases, because it neglects the vertical inertial restraint provided by the superstructure mass.

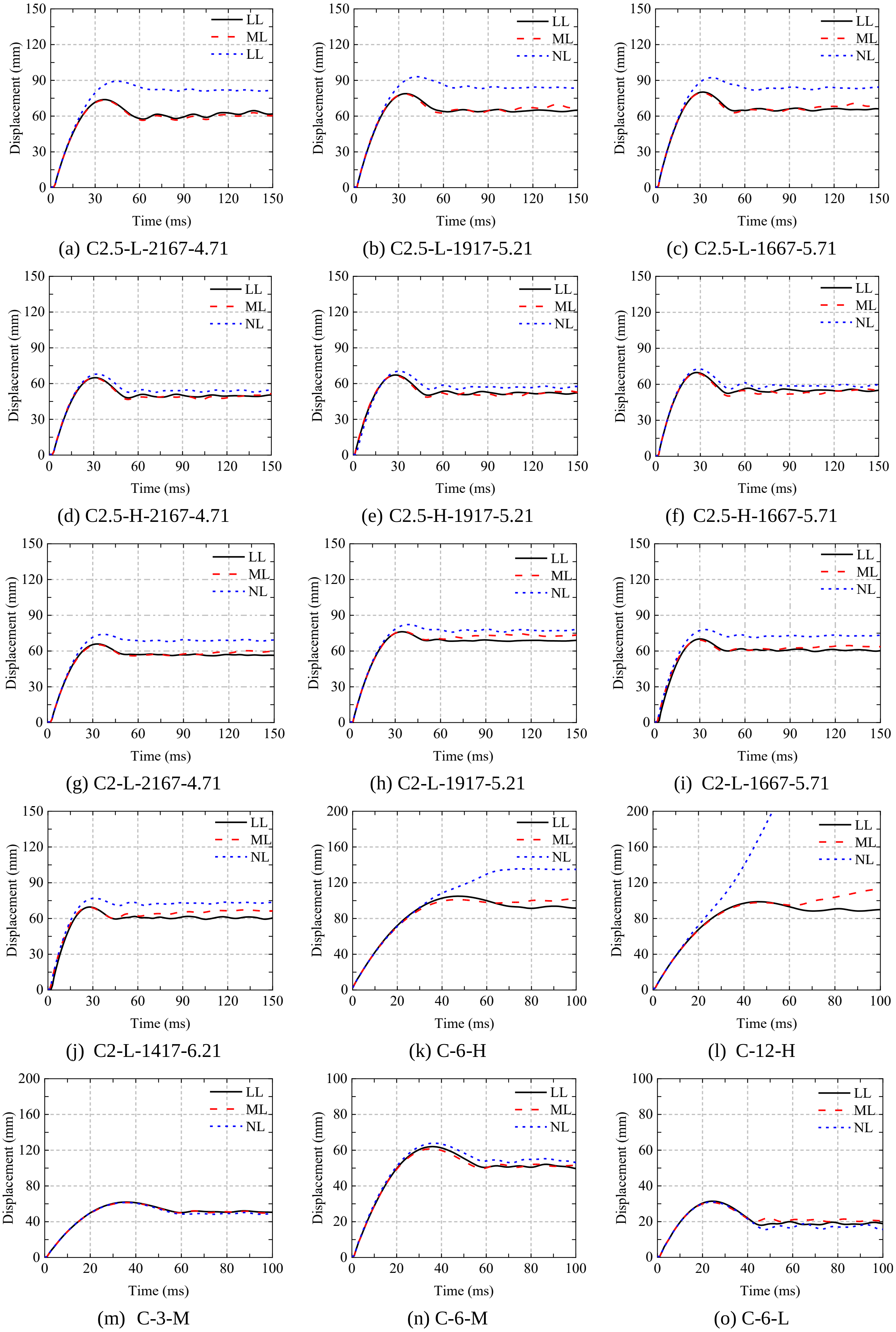

(a) C2.5-L-2167-4.71 (b) C2.5-L-1917-5.21 (c) C2.5-L-1667-5.71

(d) C2.5-H-2167-4.71 (e) C2.5-H-1917-5.21 (f) C2.5-H-1667-5.71

(g) C2-L-2167-4.71 (h) C2-L-1917-5.21 (i) C2-L-1667-5.71

(j) C2-L-1417-6.21 (k) C-6-H (l) C-12-H

(m) C-3-M (n) C-6-M (o) C-6-L

Fig. 11 Comparison of displacement time-history curves among LL, ML, and NL

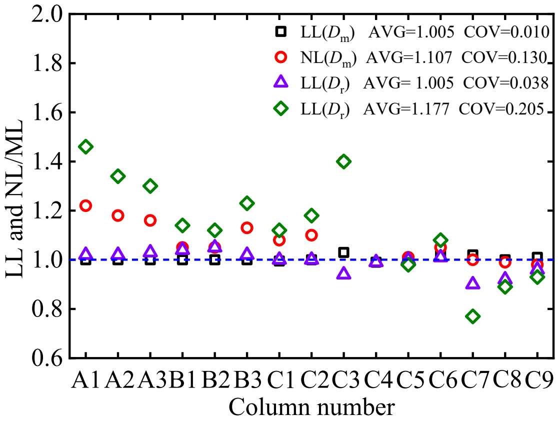

Fig. 12 Comparison of loading behavioral differences among LL, NL, and ML in terms of D_m and D_r

Fig. 12 further confirms these differences. For the LL model relative to the ML model, the mean ratios for Dm and Dr are both 1.005, with coefficients of variation of 0.010 and 0.038, respectively, indicating high consistency. In contrast, the corresponding mean ratios for the NL model are 1.107 and 1.177, with coefficients of variation of 0.130 and 0.205, respectively. This indicates that the NL model has a stronger influence on residual displacement than on peak displacement. Therefore, neglecting superstructure inertia may lead to an overestimation of irreversible post-impact deformation, especially for shear-dominated failure modes.

From an engineering perspective, the approximately 10.7% increase in peak displacement predicted by the NL model indicates a higher deformation demand during impact, which may influence structural safety when the column is close to its deformation capacity. The approximately 17.7% increase in residual displacement is more directly related to post-impact serviceability, repairability, and collapse-prevention assessment, because residual deformation reduces the remaining alignment, load-carrying stability, and post-event usability of the column. Therefore, the ML model is recommended for structural impact analyses in which the inertial participation of the upper structure and post-impact residual performance are of concern. The constant-force model does not necessarily provide conservative predictions because it may underestimate the impact-force plateau while overestimating residual deformation, leading to a biased assessment of both force demand and damage state.

4.4 Effects of Damage States and Failure Modes

Fig. 13 compares the final damage states of the 15 RC column cases predicted by the LL, ML, and NL models. The damage contours reflect the main failure characteristics under lateral impact, including local concrete crushing, diagonal damage propagation, localized shear failure, and global flexural deformation. Overall, the predicted damage is concentrated within and around the impact region, indicating that local compression and impact-induced shear concentration dominate the initial damage development of RC columns.

As shown in Fig. 13(a)–(j), the specimens in Groups A, B, and C exhibit different degrees of local damage concentration and diagonal damage propagation. For Group A, all three models predict clear impact-region damage and diagonal damage development, but the NL model shows a different extent of damage from the LL and ML models. For Group B, the damage extends not only around the impact region but also along the column height, reflecting the combined effect of global deformation and local damage. For Group C, a more pronounced damage band forms near the impact region and propagates diagonally in some cases, indicating a transition from local compression damage to coupled flexure–shear damage. In these cases, the LL and ML models provide similar damage predictions, whereas the NL model tends to produce more localized damage concentration.

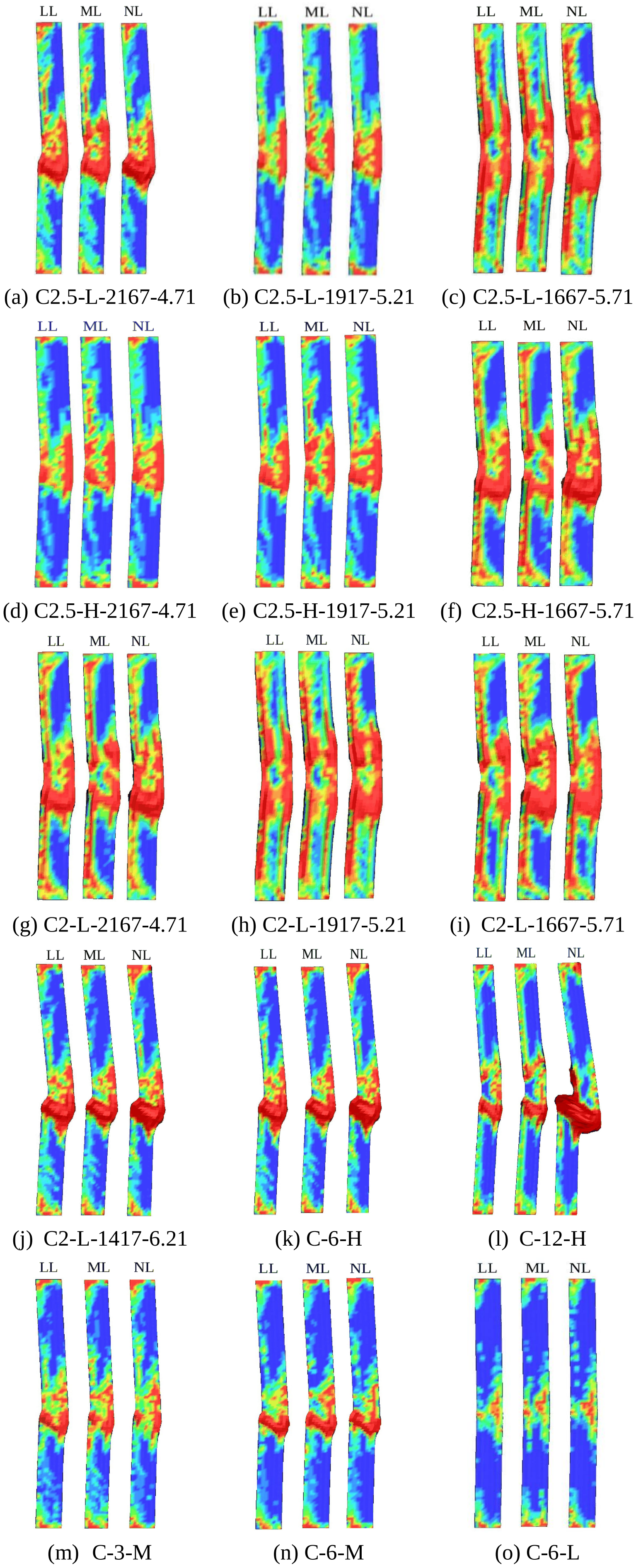

(a) C2.5-L-2167-4.71 (b) C2.5-L-1917-5.21 (c) C2.5-L-1667-5.71

(d) C2.5-H-2167-4.71 (e) C2.5-H-1917-5.21 (f) C2.5-H-1667-5.71

(g) C2-L-2167-4.71 (h) C2-L-1917-5.21 (i) C2-L-1667-5.71

(j) C2-L-1417-6.21 (k) C-6-H (l) C-12-H

(m) C-3-M (n) C-6-M (o) C-6-L

Fig. 13 Comparison of final damage states among LL, NL, and ML

Fig. 13(k)–(o) further show that the influence of axial loading models is strongly failure-mode dependent. For specimens dominated by flexural deformation, the differences among the three models are relatively small. However, for shear-controlled or flexure–shear-controlled specimens, particularly under high axial compression or severe shear damage, the NL model predicts more pronounced local crushing and damage propagation. From a mechanical perspective, shear damage is more sensitive to axial force fluctuations and compression–shear interaction than flexural damage. Therefore, neglecting superstructure inertia may lead to biased predictions of damage evolution and residual failure states, particularly for shear-controlled impact scenarios.

5. Conclusions

This study investigated the influence of axial loading models on the lateral impact response and failure prediction of axially loaded RC columns using a refined LS-DYNA finite element model. The main conclusions are as follows:

(1) The sensor-measured impact force should be corrected by considering the inertial contribution of the hammer head mass, which improves the consistency between the experimental and numerical contact forces.

(2) The validated finite element model successfully reproduces the impact force, displacement response, axial force fluctuation, and main damage patterns of RC columns under lateral impact.

(3) The axial loading model has little effect on the initial impact force peak, which is mainly controlled by local contact stiffness, impact mass, impact velocity, and concrete compression in the contact region.

(4) The axial loading representation significantly affects the impact plateau and duration. Compared with the ML model, the NL model underestimates the impact force plateau, with an average ratio of approximately 0.876.

(5) The NL model overestimates the peak and residual displacements, with average ratios of 1.107 and 1.177 relative to the ML model, respectively, demonstrating that neglecting superstructure inertia may lead to inaccurate evaluation of post-impact deformation.

(6) The influence of axial loading models is failure-mode dependent. For shear-controlled and flexure–shear-controlled columns, the ML model or an explicit superstructure mass model is recommended instead of a constant axial force boundary condition. For engineering impact simulations, the constant-force model may be acceptable for preliminary analysis of flexure-dominated columns, but should be used with caution for shear-dominated columns and when accurate prediction of residual deformation or damage evolution is required.

6. Limitations and Future Work

It should be noted that this study still has several limitations. The impact-force correction is based on an approximate synchronous-acceleration assumption for the hammer mass system, and local high-frequency effects of the sensor–hammer assembly are not fully considered. The concrete and reinforcement models also involve simplified material assumptions, and the boundary conditions were idealized according to the available test setup. In addition, the investigated cases were limited to validated test-scale column specimens. Therefore, caution should be exercised when extending the conclusions to full-scale structures, and further studies should consider different structural scales, connection details, and superstructure systems.

Acknowledgment

The study was funded by the Science and Technology Project of Housing and Urban-Rural Construction of Shandong Province (Grant No. 2022-R2-7) and the Industry–University–Research Project of the Key Research and Development Program of Linyi City (Grant No. 2024010), to which the authors are grateful.

Conflicts of Interest

The authors declare no conflict of interest.

References

[1] J. Li, R. Zhang, L. Jin, D. Q. Lan, and X. L. Du, “Simplified Support Reaction Profiles of RC Beams under Low-Velocity Impact: From Experimental Observations to Data-Driven Prediction,” Engineering Structures, vol. 344, article no. 121377, 2025.

[2] X. H. Bao, D. C. Li, D. B. Zhao, J. Shen, X. S. Chen, and H. Z. Cui, “Lateral Impact Responses of Inclined Steel-Reinforced Concrete Column: Experimental and Numerical Investigations,” Structures, vol. 74, article no. 108601, 2025.

[3] J. H. Wei, J. Y. Xue, Z. B. Hu, L. Qi, and J. Xu, “Dynamic Response and Post-Impact Damage Assessment of Steel Reinforced Concrete Columns under Lateral Impact Loads,” Engineering Structures, vol. 328, article no. 119735, 2025.

[4] J. Jiang and A. D. Sorensen, “Finite Element Analysis of Reinforced Concrete Bridge Piers under Sequential Vehicle Impact and Seismic Loads: Case Study,” Transportation Research Record, vol. 2679, no. 10, pp. 430-448, 2025.

[5] Y. Y. Mo, Y. L. Han, J. Zhang, Z. Y. Zhang, and W. D. Wu, “Dynamic Response Analysis of Hollow Thin-Walled Pier Rigid-Frame Bridge under Rockfall Impacts,” Advances in Bridge Engineering, vol. 6, article no. 30, 2025.

[6] S. U. Azunna, F. N. A. A. Aziz, and R. S. M. Rashid, “Dynamic Response of Rubberized Geopolymer Concrete Column Subjected to Lateral Impact,” Progress in Engineering Science, vol. 2, no. 3, article no. 100130, 2025.

[7] J. M. Sun, H. Chen, F. Yi, Y. B. Ding, Y. Zhou, Q. F. He, et al., “Experimental and Numerical Study on Influence of Impact Mass and Velocity on Failure Mode of RC Columns under Lateral Impact,” Engineering Structures, vol. 314, article no. 118416, 2024.

[8] A. Cengiz, T. Gurbuz, A. Ilki, and M. Aydogan, “Dynamic and Residual Static Behavior of Axially Loaded RC Columns Subjected to Low-Elevation Impact Loading,” Buildings, vol. 14, no. 1, article no. 92, 2024.

[9] S. Karunarathna, S. Linforth, A. Kashani, X. Liu, and T. Ngo, “Numerical Investigation on the Behaviour of Concrete Barriers Subjected to Vehicle Impacts Using Modified K&C Material Model,” Engineering Structures, vol. 308, article no. 117943, 2024.

[10] A. Chen, Y. Liu, R. Ma, and X. Zhou, “Experimental and Numerical Analysis of Reinforced Concrete Columns under Lateral Impact Loading,” Buildings, vol. 13, no. 3, article no. 708, 2023.

[11] K. Al-Bukhaiti, Y. Liu, S. Zhao, H. Abas, D. Han, N. Xu, et al., “Effect of the Axial Load on the Dynamic Response of the Wrapped CFRP Reinforced Concrete Column under the Asymmetrical Lateral Impact Load,” PLoS ONE, vol. 18, no. 6, article no. e0284238, 2023.

[12] H. X. Luan, J. Wu, T. B. Cao, X. Zhao, F. Geng, and G. Q. Dong, “Axial Compression Performance of Reinforced Concrete Columns after Lateral Impact Load,” KSCE Journal of Civil Engineering, vol. 27, no. 8, pp. 3528-3541, 2023.

[13] Y. C. Song, J. J. Wang, and Q. Han, “Dynamic Performance of Flexure-Failure-Type Rectangular RC Columns under Low-Velocity Lateral Impact,” International Journal of Impact Engineering, vol. 175, article no. 104541, 2023.

[14] J. H. Zhong, C. M. Song, J. W. Xu, Y. H. Cheng, and F. Liu, “Experimental and Numerical Simulation Study on Failure Mode Transformation Law of Reinforced Concrete Beam under Impact Load,” International Journal of Impact Engineering, vol. 179, article no. 104645, 2023.

[15] Z. Luo and Y. H. Wang, “Experimental and Numerical Study of Axially Loaded Reinforced Concrete Columns and Frame Columns under Lateral Impact Loading,” Canadian Journal of Civil Engineering, vol. 49, no. 3, pp. 330-345, 2022.

[16] H. W. Li, W. S. Chen, Z. J. Huang, H. Hao, T. T. Ngo, and T. M. Pham, “Influence of Various Impact Scenarios on the Dynamic Performance of Concrete Beam-Column Joints,” International Journal of Impact Engineering, vol. 167, article no. 104284, 2022.

[17] W. C. Zhao and J. H. Ye, “Dynamic Behavior and Damage Assessment of RC Columns Subjected to Lateral Soft Impact,” Engineering Structures, vol. 251, part A, article no. 113476, 2022.

[18] H. W. Li, W. S. Chen, T. M. Pham, H. Hao, and T. T. Ngo, “Analytical and Numerical Studies on Impact Force Profile of RC Beam under Drop Weight Impact,” International Journal of Impact Engineering, vol. 147, article no. 103743, 2021.

[19] C. W. Zhang, G. Gholipour, and A. A. Mousavi, “State-of-the-Art Review on Responses of RC Structures Subjected to Lateral Impact Loads,” Archives of Computational Methods in Engineering, vol. 28, no. 4, pp. 2477-2507, 2021.

[20] H. W. Li, W. S. Chen, and H. Hao, “Factors Influencing Impact Force Profile and Measurement Accuracy in Drop Weight Impact Tests,” International Journal of Impact Engineering, vol. 145, article no. 103688, 2020.

[21] W. C. Zhao and J. Qian, “Resistance Mechanism and Reliability Analysis of Reinforced Concrete Columns Subjected to Lateral Impact,” International Journal of Impact Engineering, vol. 136, article no. 103413, 2020.

[22] J. M. Sun, W. J. Yi, H. Chen, F. Peng, Y. Zhou, and W. X. Zhang, “Dynamic Responses of RC Columns under Axial Load and Lateral Impact,” Journal of Structural Engineering, vol. 149, no. 1, article no. 04022210, 2023.